Appendix

Q1 (c).

(i) Velocity manipulability ellipse plot as well as force manipulability ellipse plot (along the Cartesian X-Z plane) for the robot at different joint postures.

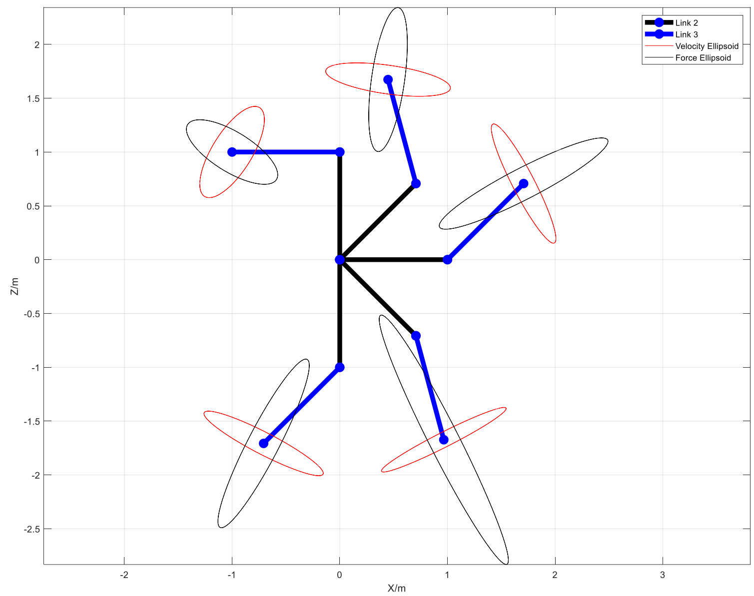

Fig. 1 Manipulability ellipse

Q2 (a). Simulation results about the tracking error of the tip ||xerror|| and the evolution of joint angles and joint velocities. (The initial state is $q_0 = [0 \quad -\pi/2 \quad \pi/2]^T$).

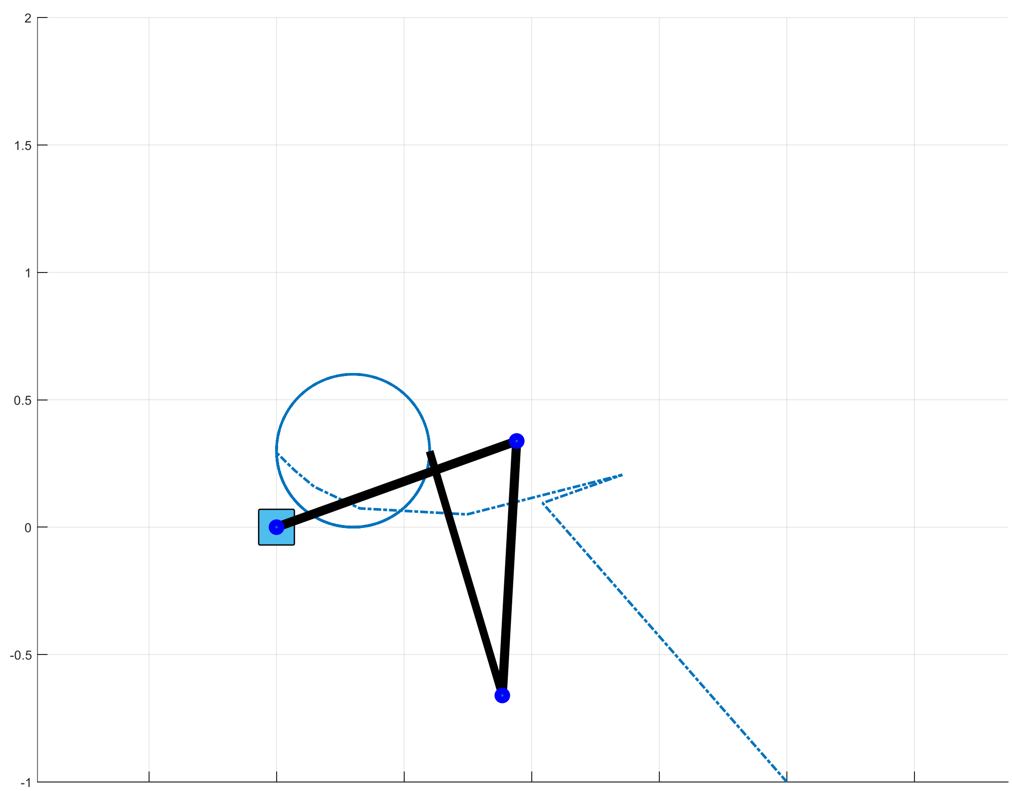

Fig. 2 Pseudoinverse Tracking Trajectory

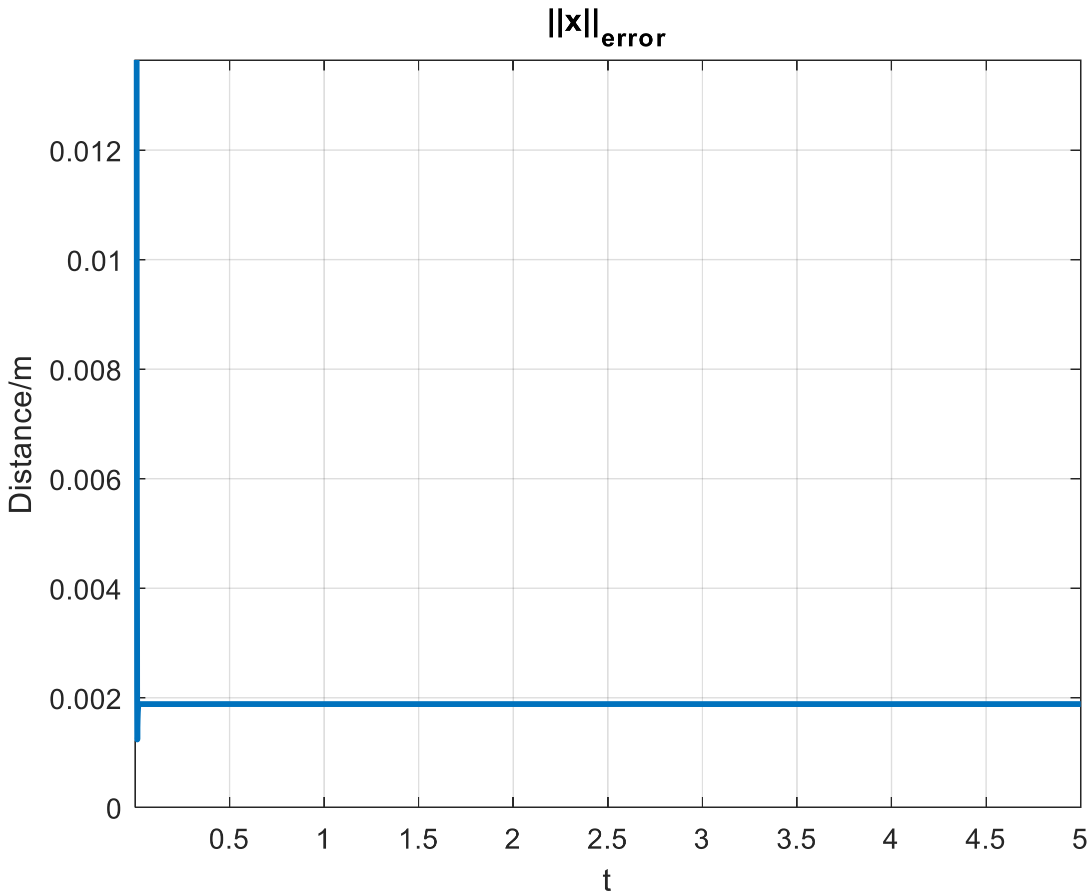

Fig. 3 Pseudoinverse Tracking error of the tip

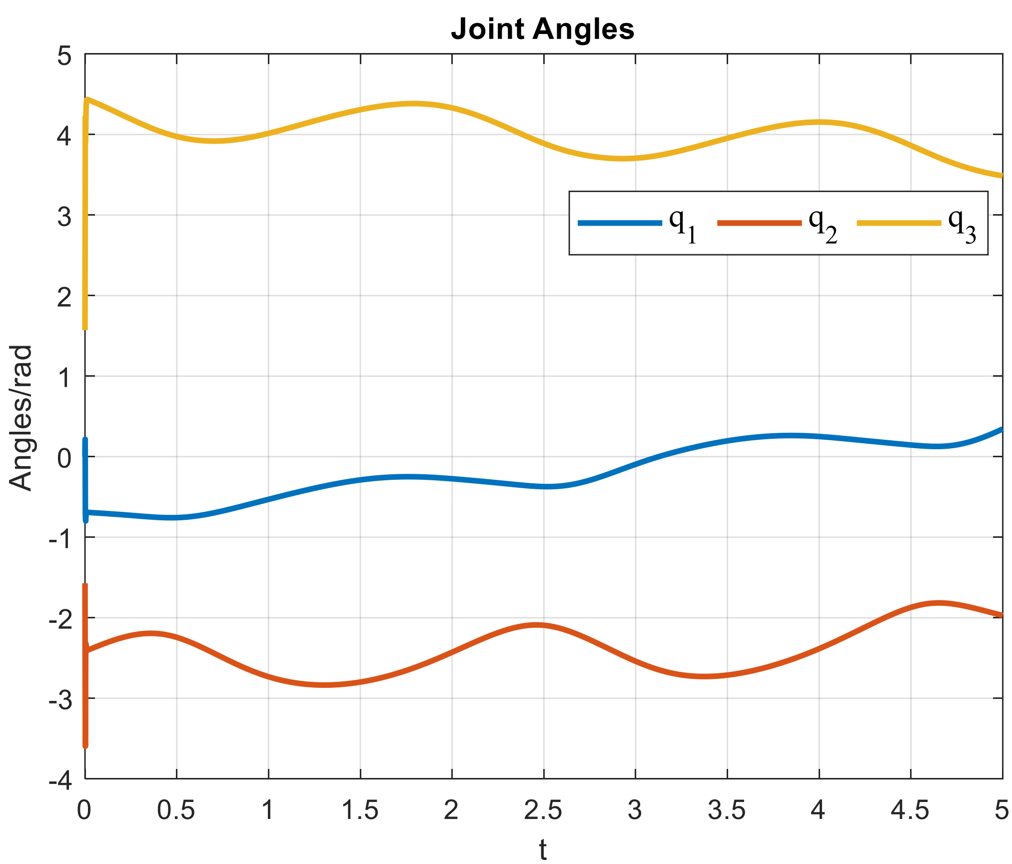

Fig. 4 Pseudoinverse Joint angles

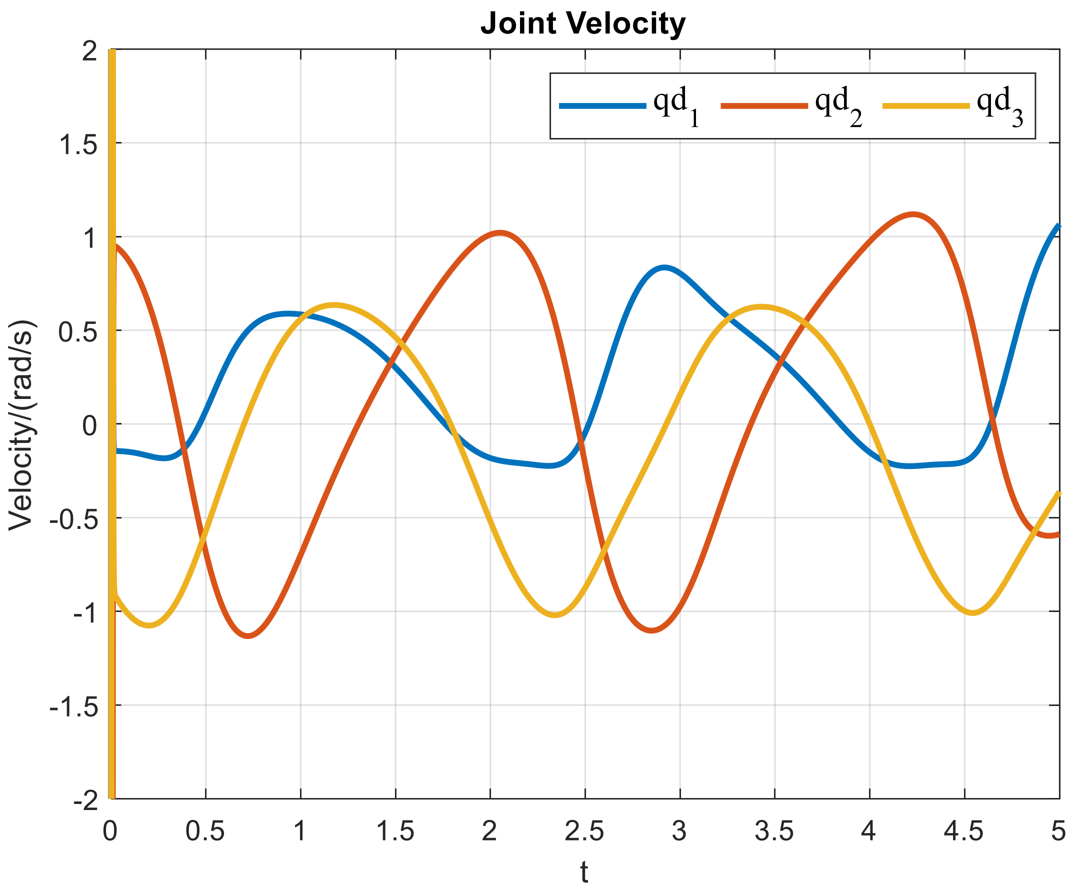

Fig. 5 Pseudoinverse Joint Velocity

Q2 (b). Vary the magnitude of the gain matrix by 50%, 200%, and 500 %. (The initial state is $q_0 = [0 \quad -\pi/2 \quad \pi/2]^T$).

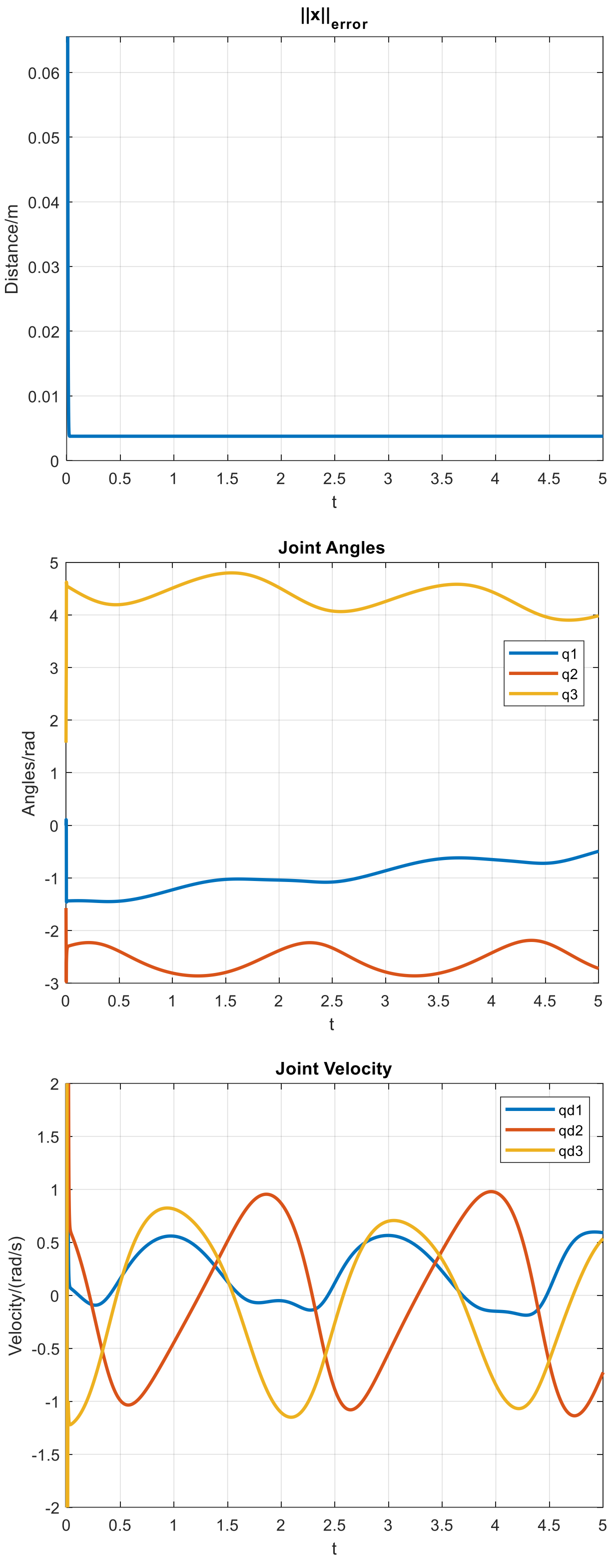

Fig 6. 50% gains

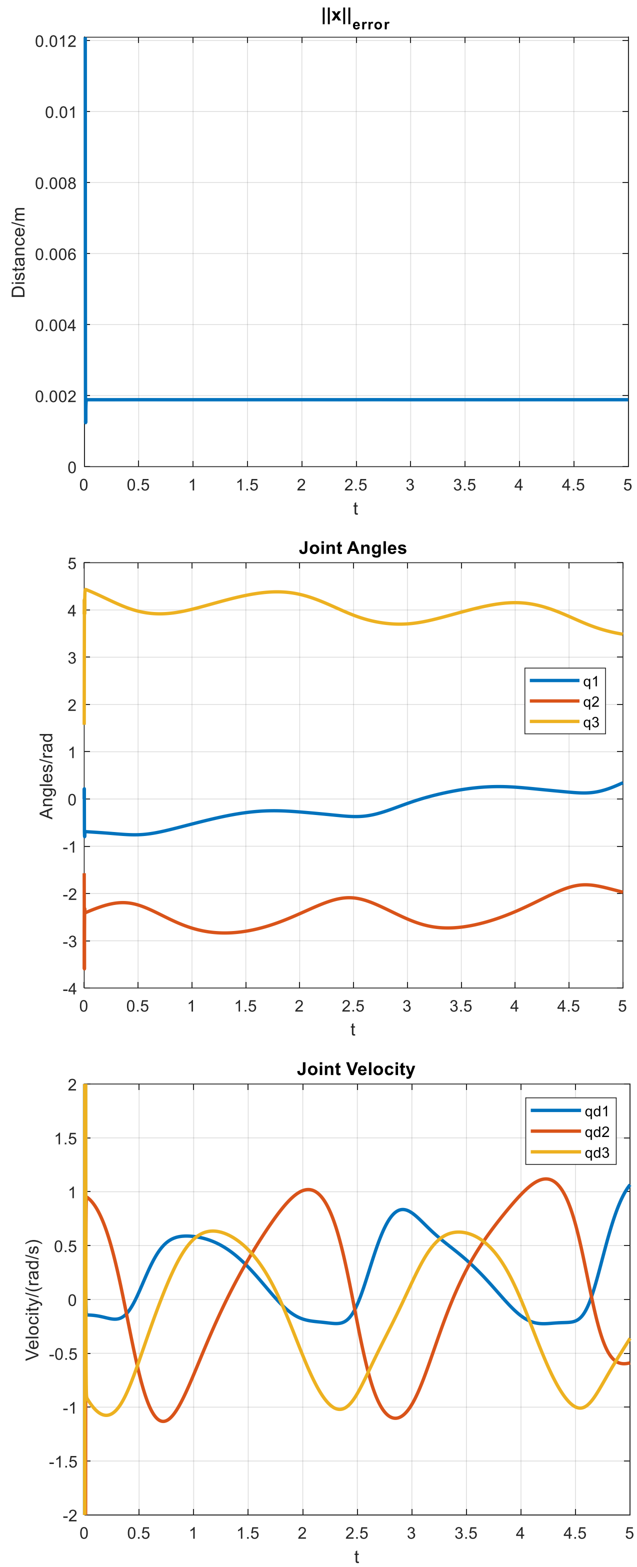

Fig 7. 100% gains

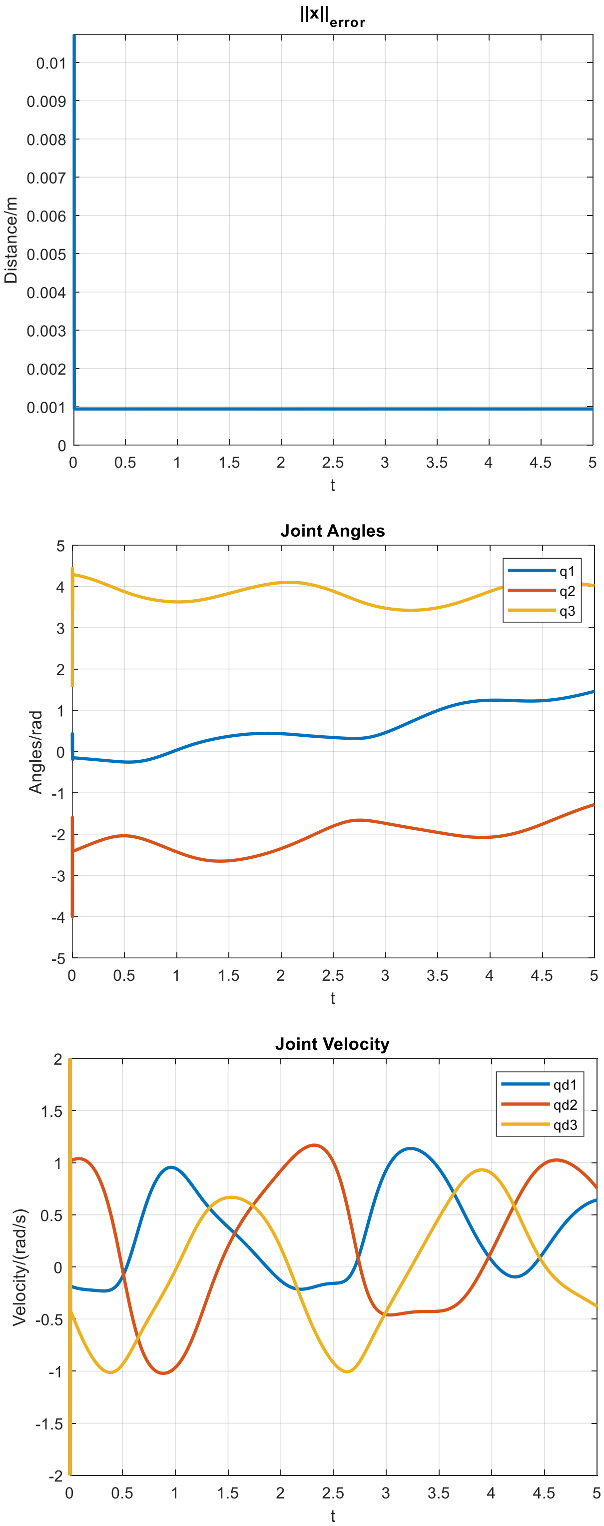

Fig 8. 200% gains

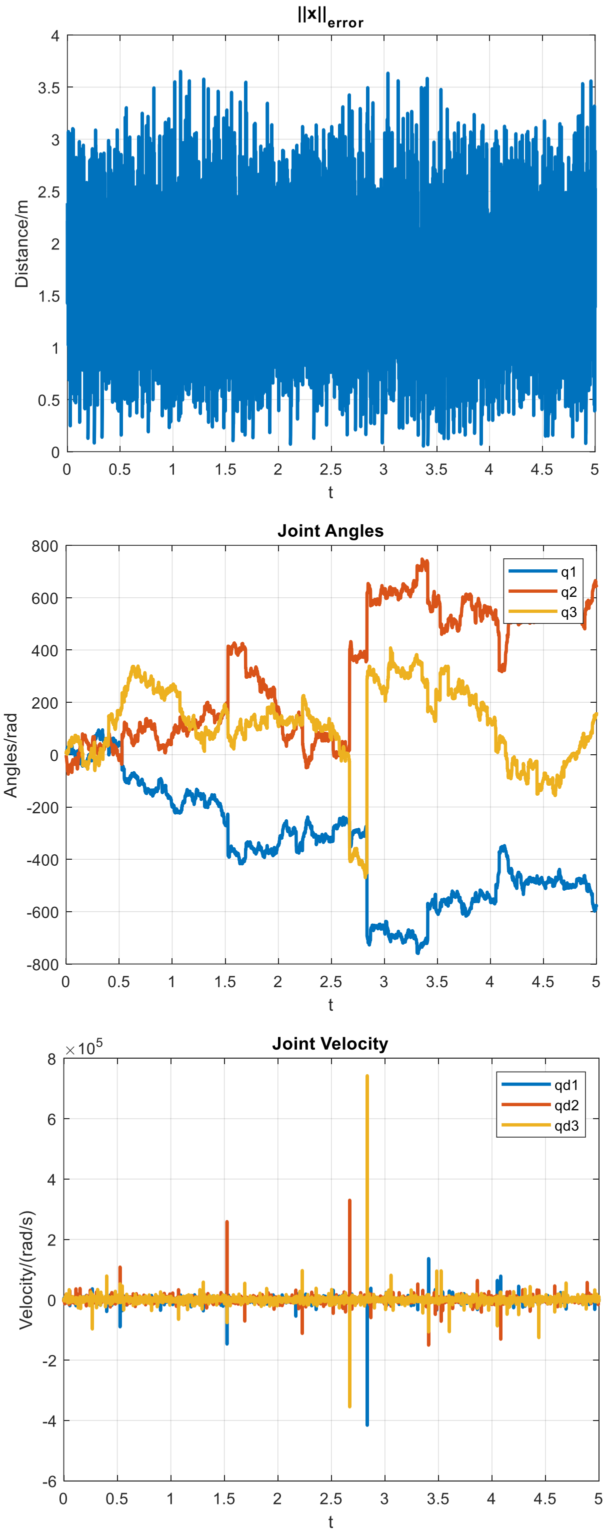

Fig 9. 500% gains

Compared Fig. 6, Fig. 7 and Fig. 8, we can see when the gain matrix gets larger, the $||x||_{error}$ becomes smaller. Especially, $||x||_{error} \approx 0.001m$ with 200% of K. But, the kinematics closed loop will not converge if eigenvalues of K are larger than ${}^{1}/_{\Delta t}$ as shown in Fig. 9.

Q2 (c). (Weighted Pseudoinverse) Create a weighted matrix to minimize the velocity of the first joint of the robot. (The weighted matrix is $W = \mathrm{daig}(4,1,1)$. In the same simulation conditions as (a) part, turn the Pseudoinverse into Weighted Pseudoinverse. The simulation results are as below.)

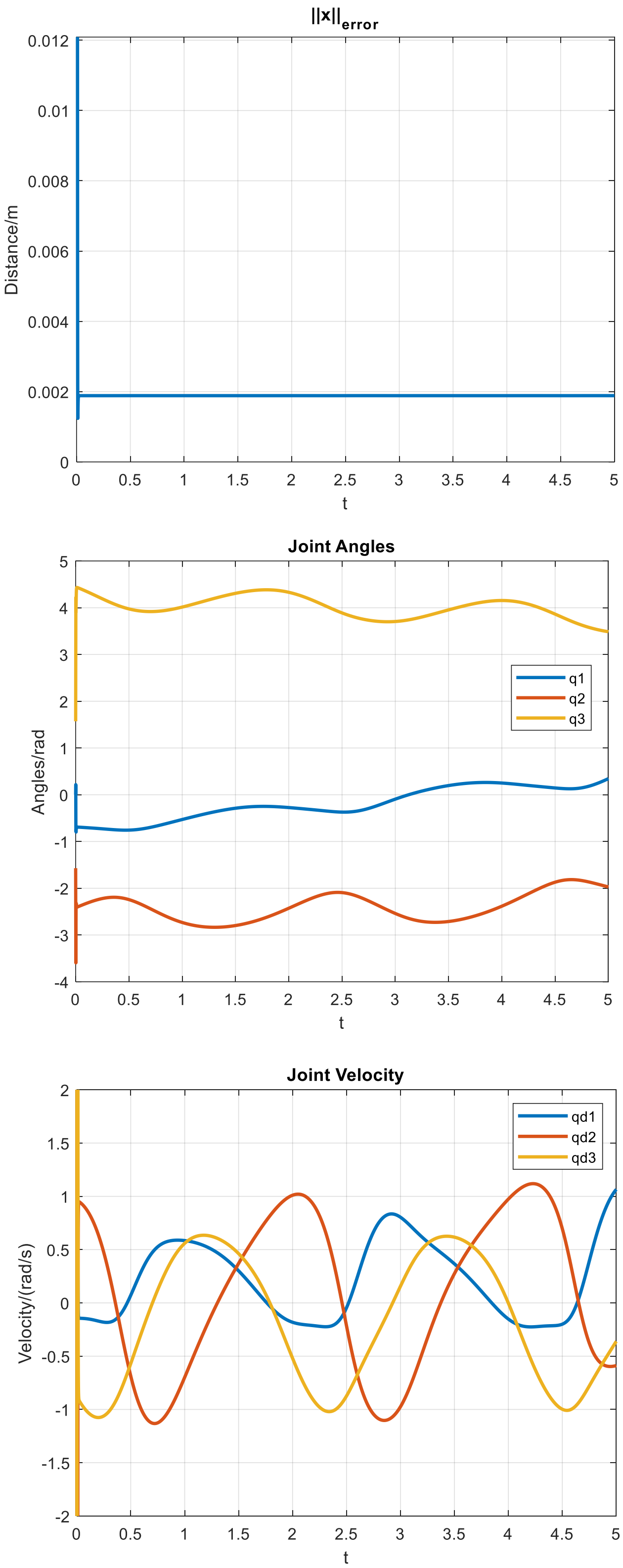

Fig. 10 Pseoinverse Simulations

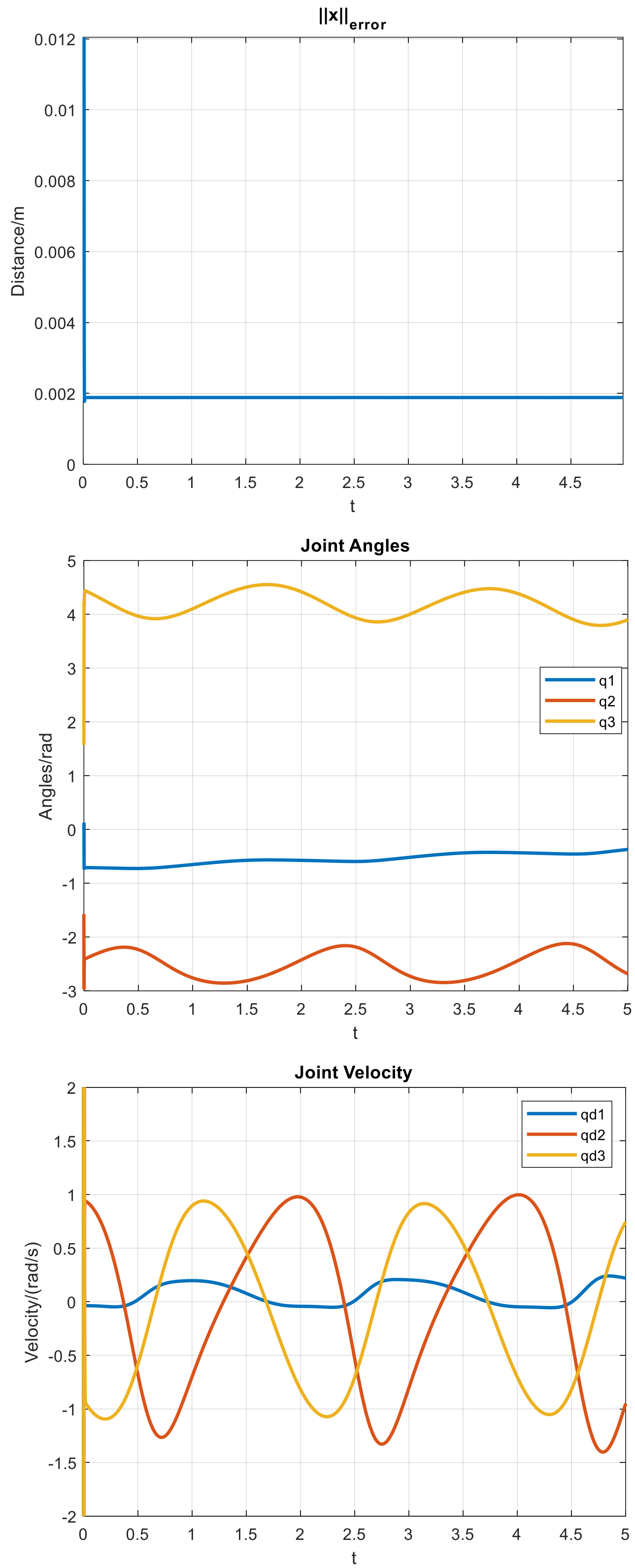

Fig. 11 Weighted Pseoinverse Simulations

Compared Fig. 11 with Fig. 10, q_{d1} in Fig. 11 is nearly half of q_{d1} in Fig. 10, which shows the Weighted Matrix has successfully minimized the velocity of the first joint of the robot.

Q2 (d)(v). Maximize the manipulability.

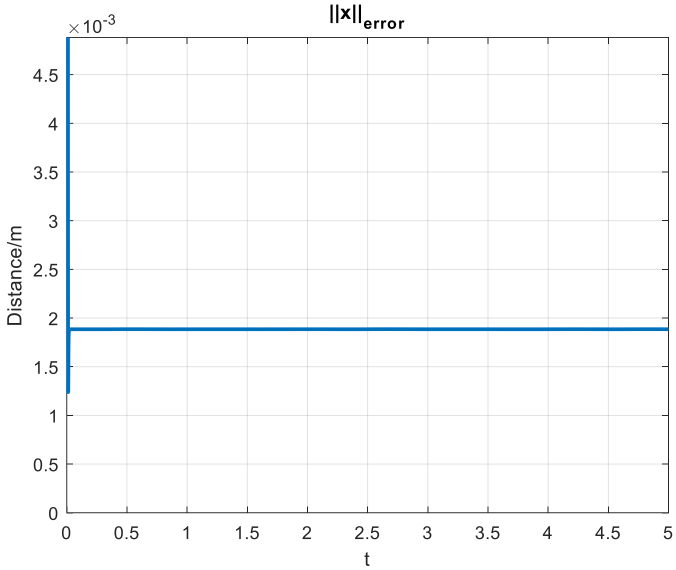

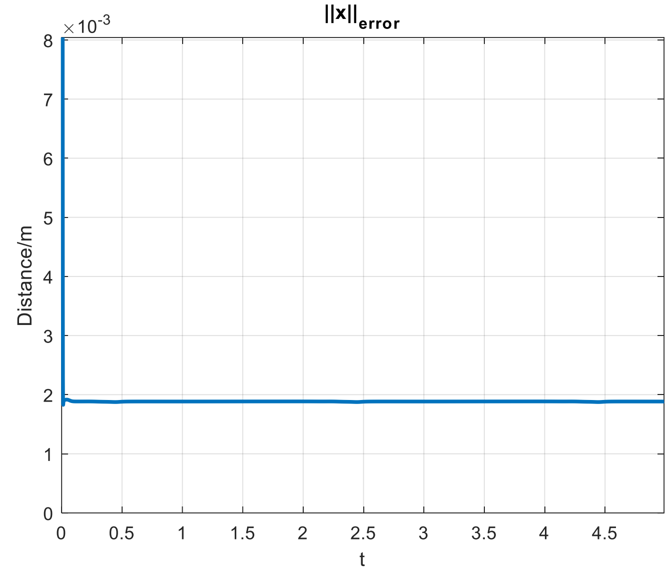

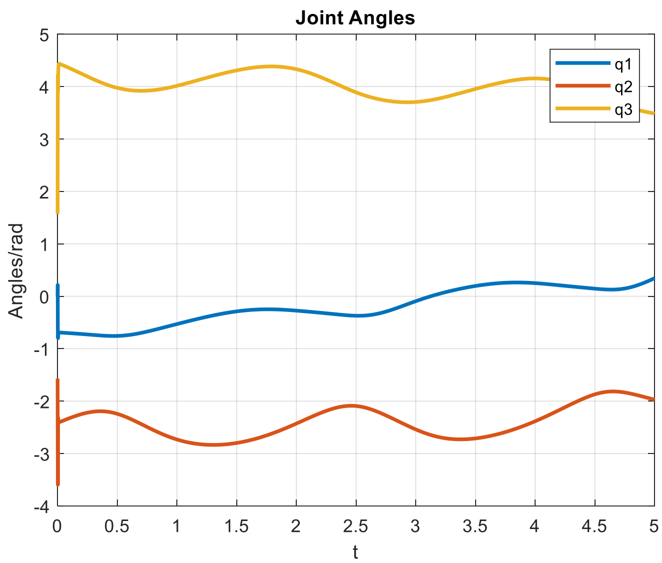

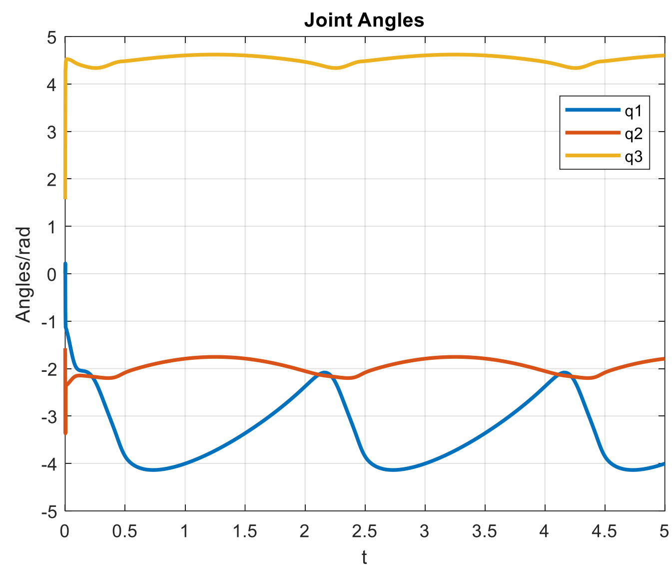

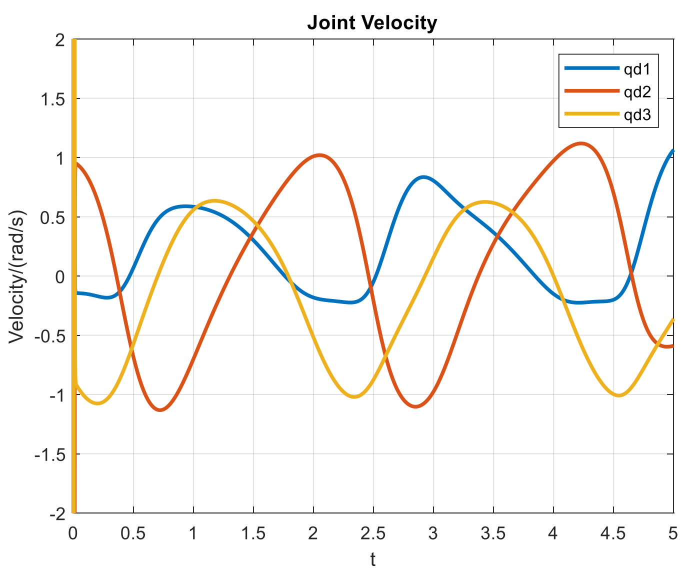

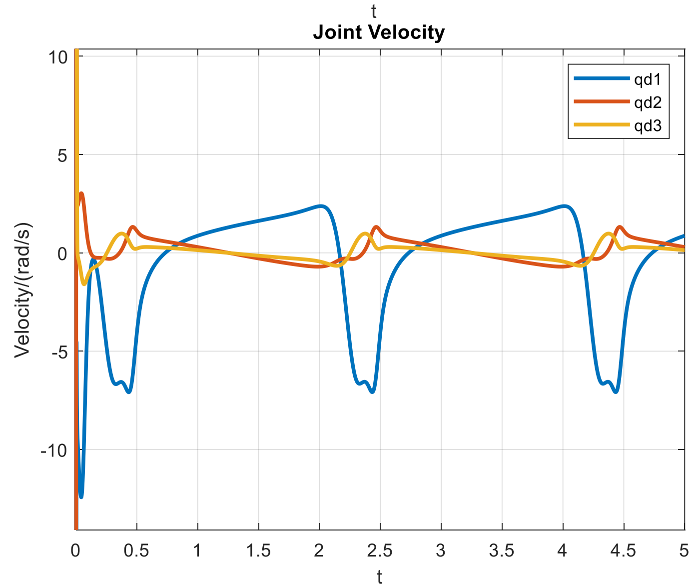

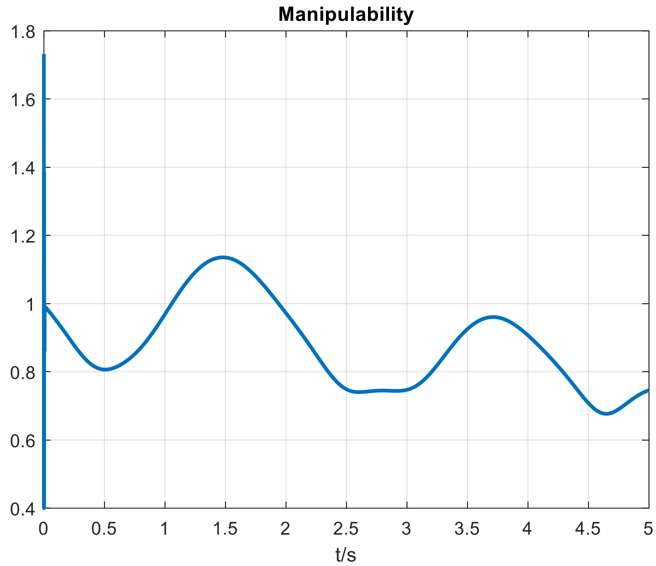

Fig. 12 Pseoinverse Simulations

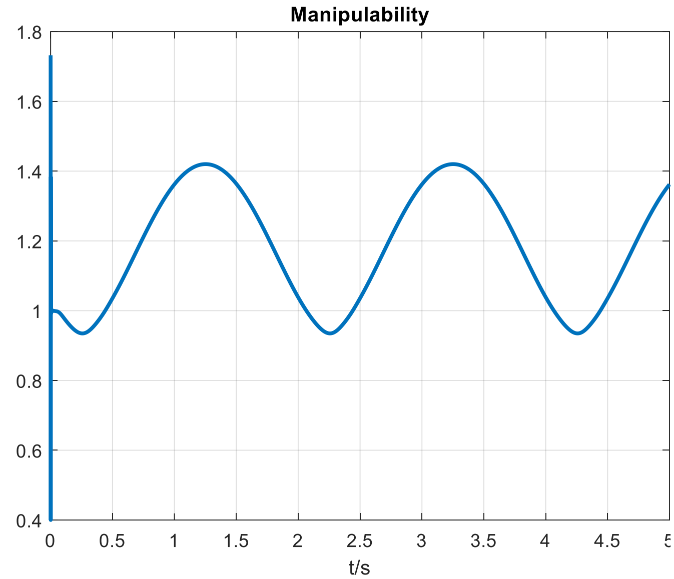

Fig. 13 Maximize the manipulability Simulations

Compared Fig. 13 with Fig. 12, it is obvious that the manipulability has been largely improved using null space projection approach.

Q2 (d)(vi). Maximize the distance from the mechanical joint limits. (The mechanical joint limits are $q_1 \in [0, 2\pi]$, $q_2 \in [-\pi, \pi]$, $q_3 \in [0, 2\pi]$, and change the initial state $q_0 = [\pi \quad -\pi/4 \quad \pi/2]^T$)

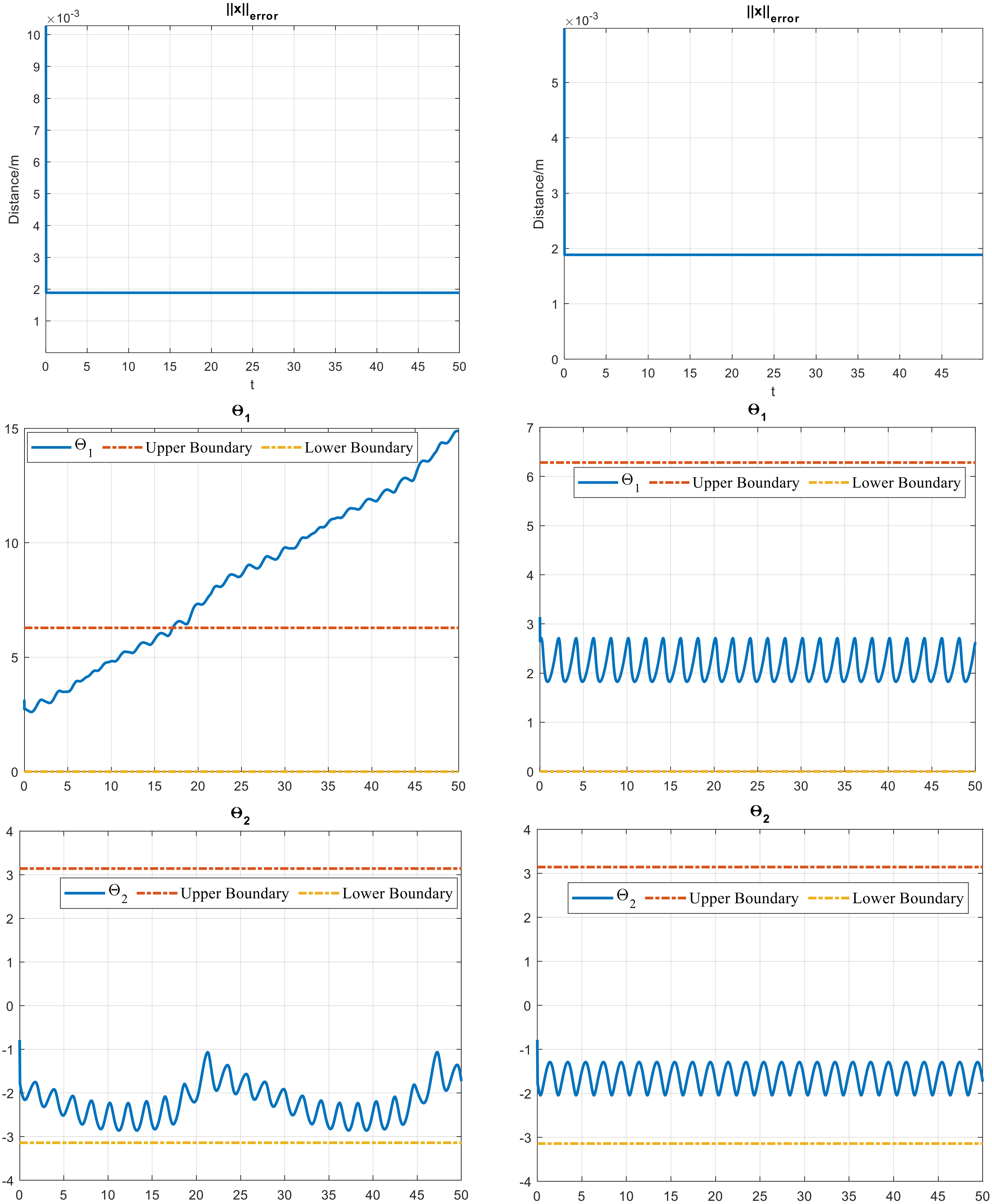

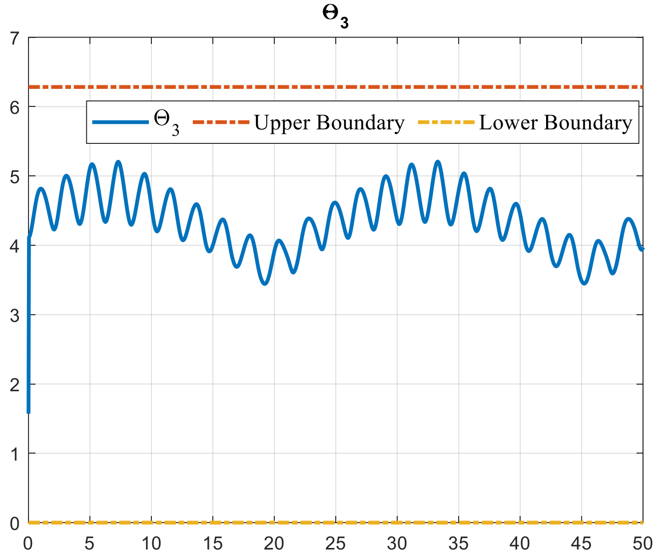

Fig. 13 Pseudoinverse Solution

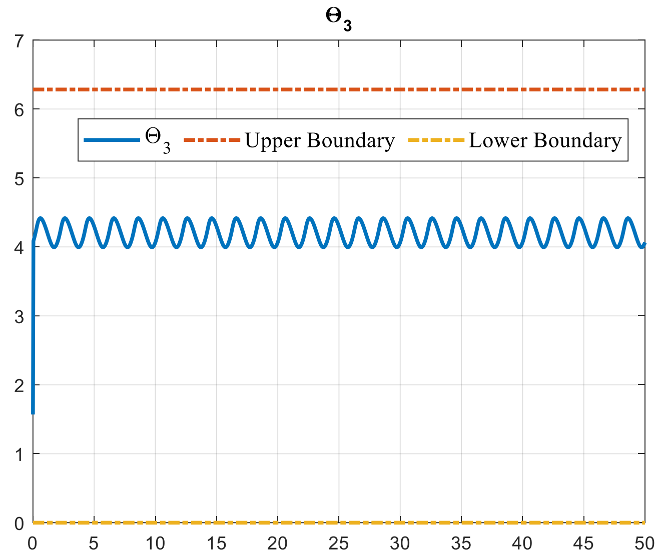

Fig. 14 Maximize the distance from the mechanical joint limits

Rather than applying the cost function mentioned in the lecture $\mathrm{w(q)} = -\frac{1}{2}(q-\bar{q})^T(q-\bar{q})$ here, I choose to apply the cost function $\mathrm{w(q)} = -\sum_{i=1}^{n}\frac{1}{4}\frac{(q_{max}-q_{min})^2}{(q_{max}-q_i)(q_i-q_{min})}$, which could make the system converge more quickly especially when the joint is reaching the limits. As Fig. 14 shows, $\boldsymbol{q_1}$ has been successfully bounded between $[\mathbf{0}, \mathbf{2\pi}]$. While $\boldsymbol{q_2}$ and $\boldsymbol{q_3}$ are more stable in their respective joint limits. Also, the error is quite acceptable by using null space projection approach.